



HAL
open science

FIBER-ML, an Open-Source Supervised Machine Learning Tool for Quantification of Fibrosis in Tissue Sections

Caterina Facchin, Anais Certain, Thulaciga Yoganathan, Clement Delacroix, Alicia Arevalo Garcia, François Gaillard, Olivia Lenoir, Pierre-Louis Tharaux, Bertrand Tavitian, Daniel Balvay

► **To cite this version:**

Caterina Facchin, Anais Certain, Thulaciga Yoganathan, Clement Delacroix, Alicia Arevalo Garcia, et al.. FIBER-ML, an Open-Source Supervised Machine Learning Tool for Quantification of Fibrosis in Tissue Sections. *American Journal of Pathology*, 2022, 192 (5), pp.783-793. 10.1016/j.ajpath.2022.01.013 . inserm-03788337

HAL Id: inserm-03788337

<https://inserm.hal.science/inserm-03788337>

Submitted on 22 Jul 2024

HAL is a multi-disciplinary open access archive for the deposit and dissemination of scientific research documents, whether they are published or not. The documents may come from teaching and research institutions in France or abroad, or from public or private research centers.

L'archive ouverte pluridisciplinaire **HAL**, est destinée au dépôt et à la diffusion de documents scientifiques de niveau recherche, publiés ou non, émanant des établissements d'enseignement et de recherche français ou étrangers, des laboratoires publics ou privés.



Distributed under a Creative Commons Attribution - NonCommercial 4.0 International License

FIBER-ML, an open-source supervised machine learning tool for quantification of fibrosis in tissue sections.

Short running title: **FIBER-ML for fibrosis quantification.** Caterina Facchin^{1,*}, Anais Certain^{1,*}, Thulaciga Yoganathan¹, Clement Delacroix¹, Alicia Arevalo Garcia¹, François Gaillard¹, Olivia Lenoir¹, Pierre-Louis Tharaux¹, Bertrand Tavitian^{1,2} and Daniel Balvay^{1,2}

¹ Université de Paris, INSERM, PARCC, F-75006 Paris, France

² Radiology Department, APHP, Hopital Européen Georges Pompidou, F-75015 Paris

Corresponding authors: - Daniel Balvay

Paris Cardiovascular Research Center (PARCC)

UMR970 INSERM / Université de Paris

Paris, France

daniel.balvay@inserm.fr

- Caterina Facchin

McGill University Health Center (RI-MUHC), 1001 Decarie Blvd,

Research Institute, Montreal, QC H4A 3J1, Canada

caterina.facchin@mail.mcgill.ca

Number of text pages: 28; Tables: 2; Figures Legends: 4; Supplementary Figures: 1.

Funding: Funding: The project was supported by an Ile-de-France region SESAME grant, the Plan Cancer Physicancer (grant C16025KS) and LABEX WIFI (Laboratory of Excellence ANR-10-LABX-24) within the French program ‘Investments for the Future’ under reference ANR-10-IDEX-0001-02 PSL. *In vivo* imaging was performed at the Life Imaging Facility of Paris Descartes University (Plateforme Imageries du Vivant - PIV), supported by France Life Imaging (grant ANR-11-INBS-0006) and Infrastructures Biologie-Santé. CF was supported by a scholarship from the Ministère de l’Enseignement Supérieur et de la Recherche. AC was supported by grants from Plan Cancer. This project has received funding from the Euratom research and training programme 2014-2018 under grant agreement No 755523. Funding from the Paradifference Foundation and the Cancer Research for Personalized Medicine - CARPEM project (Site de Recherche Intégré sur le Cancer - SIRIC) is gratefully acknowledged.

Competing interests: The authors declare no competing interests.

* These authors contributed equally to this work

† Present address: McGill University Health Center (RI-MUHC), 1001 Decarie Blvd, Research Institute, Montreal, QC H4A 3J1, Canada

ABSTRACT

Pathological fibrosis is a major hallmark of tissue insult in many chronic diseases. Although the amount of fibrosis is recognized as a direct indicator of disease extension, there is no consensus method for its quantification on tissue sections. Here, we tested “FIBER-ML,” a semi-automatic, free and open-source software, that uses a machine-learning approach to quantify fibrosis automatically after a short user-controlled learning phase. Fibrosis was quantified in Sirius Red-stained tissue sections from two fibrogenic animal models: (i) acute stress-induced cardiomyopathy in rats (Takotsubo syndrome-like (TTS)) and (ii) Human Immunodeficiency Virus - induced nephropathy in mice (chronic kidney disease (CKD)). In TTS, FIBER-ML 1.0 was compared with ImageJ. In CKD, it was compared with the commercial inForm software. Intra-operator, inter-operator, inter-software correlations and agreements were assessed. All correlations (r) were excellent ($r > 0.95$) in both datasets. The discriminatory power (d) between pathological and healthy groups were $d < 10^{-3}$ for TTS and $d < 10^{-4}$ for CKD data. Intra-operator agreements, assessed by intraclass coefficient correlation (ICC), were good ($ICC > 0.8$), while inter-operator and inter-software agreements ranged from moderate to good ($ICC > 0.7$). FIBER-ML performed fast, user-friendly, reproducible and consistent quantification of fibrosis in tissue sections. It offers an open-source alternative to current software, including quality controls and file management.

INTRODUCTION

Tissue fibrosis is defined by deposits of extracellular matrix (ECM) components, such as collagen. Although fibrosis is a natural response to tissue lesions and is essential for scar formation, diffuse interstitial and perivascular/periglomerular fibrosis are detrimental to tissue physiology and may lead to organ failure. Pathological fibrosis is induced by chronic inflammation states [1] triggered by a variety of mechanical and chemical stimuli [2] and results in the activation of a complex cascade of cellular and molecular pathways [3]. It is observed in most tissues and organs, where it leads to a progressive modification of tissue architecture and consequent tissue dysfunction [4]. Fibrosis is a well-recognized cause of morbidity and mortality [2] in heart and kidney. Interstitial myocardial fibrosis follows myocardial infarction [5]. Perivascular fibrosis is observed in a multitude of cardiac pathologies leading to changes in myocardial load or inflammation, such as hypertensive disease or diabetic hypertrophic cardiomyopathy [6–10]. In preclinical research, histological quantification of myocardial fibrosis is extensively used for the investigation of the molecular mechanisms underlying the fibrogenic processes and the search for potential therapeutic targets [11]. Renal interstitial fibrosis is one of the most important hallmarks of progressive renal diseases, including chronic kidney disease (CKD) [12], which is a major problem in public health [13]. The amount of renal fibrosis correlates with the progressive loss of kidney function [14], and is assessed for the prognosis of kidney diseases and for the evaluation of new therapies [15–17].

While new tools as blood biomarkers and *in vivo* imaging are emerging for the evaluation of fibrosis in the kidney and heart [18–22], the histological assessment of fibrosis in kidney biopsies [16] and in post mortem cardiac tissue remains a gold standard. For clinical [23,24] as well as preclinical studies [25,26], fibrosis is usually estimated by analysis of tissue sections after Sirius Red staining, one of the most used stains because of its ability to selectively highlight collagen networks [27]. Using digital scanners, an increasing number of digital images can be recorded with color and illumination normalization [28], offering a large number of high quality images, which are

ideal for improved analysis and efficient quantification [29,30]. Software analysis saves time and decreases intra- and inter-operator variability for large volumes of data [31,32], and automation is therefore a holy grail. However, apart from highly normalized cases, over-automation can induce significant artifacts, either because the acquisition conditions were not foreseen by the software designer, or because the quantification process must rely on decisions made by the experimenter. The qualities expected from a quantification software are multiple. On the one hand, it is necessary to allow the operator to control the data processing workflow, and on the other hand it is necessary to limit the outcome variability by minimizing and simplifying the human intervention. The optimization of the operator's intervention in the workflow is critical in order to provide a qualitative input and a quality control within the analysis of large volumes of data. In all cases, the risks of loss of control of the analysis must be taken into consideration [33,34]. The software should help the operator to adjust the algorithm according to the numerous factors that affect the quality of histological staining [30,33] and provide feedbacks to the operator to control the relevance of the quantitative outcomes.

Some commercial software integrates supervised machine learning techniques. Open-source software, such as ImageJ [35,36], uses older techniques such as manual color thresholding [37] but can also integrate more recent machine learning techniques [38,39]. Many biology laboratories still use older approaches, possibly reflecting a lack of access to newer techniques. Open-source software solutions are usually less user-friendly and provide few tools, if any, to facilitate data management and quality controls. Professional programs are not available in many laboratories and their algorithms are often opaque and hard to adjust.

We have designed a new software for fibrosis quantification named “FIBER-ML”, based on a parsimonious machine learning process. FIBER-ML aims at accelerating, facilitating and providing better control of the analysis by biologists, and has been tested in research paradigms [40–42] using various staining methods. Here, we describe the methodology supporting FIBER-ML, define its

intra- and inter-operator reproducibility and its consistency with other software solutions for the quantification of fibrosis. FIBER-ML was compared to an open-source ImageJ plugin, generated from a rat model of Takotsubo Syndrome (TTS) [43] and to the commercial software inForm, from a murine model of Human Immunodeficiency Virus (HIV) associated chronic kidney disease (CKD) [44], for cardiac and renal fibrosis, respectively. As a companion tool to the present article, FIBER-ML is made available to the community both in executable and open-source formats.

MATERIAL AND METHODS

FIBER-ML 1.0 Software

FIBER-ML 1.0 was developed with Matlab (Mathworks, Natick, MA) to segment/classify histologic images in a simple and efficient way and count the number of pixels of each class. The core of FIBER-ML 1.0 consists in a learning interface and an automatic segmentation module. Learning is performed by clicking on pixels in images. The classification of the pixels is based on a low complexity classifier using the Discriminant Analysis method. FIBER-ML includes a study management module, allowing the tracing and reuse of data generated during the process, and a quality control interface. FIBER-ML can be used either via its standalone executable version or in its interpreted version, which can be run and amended using the Matlab version 2019.b or later, with adapted Image Processing and Statistics and Machine Learning toolboxes and parsed with any text editor.

Data

FIBER-ML was tested on two data sets were obtained from two studies.

Myocardial fibrosis was measured in a rat model of stress-induced cardiomyopathy (Takotsubo Syndrome - TTS) [43], inducing delayed interstitial and diffuse perivascular fibrosis in the myocardium [43,45]. Heart-stained slices were scanned with 20x mode (15 mm × 15 mm) in a NanoZoomer S210 system (Hamamatsu). The scan resolution at 20x was 0.46 µm/pixel. The accompanying software NDPview 2 allows the user to navigate through the captured Whole Slide Image (WSI) at any given digital zoom up to 40x. It resulted in a total of 42 Tiff WSI, or 14 individuals in triplicates (7 pathological, 7 controls).

Kidney fibrosis was quantified in a murine model of Human Immunodeficiency Virus (HIV) associated nephropathy [44]. HIV-associated nephropathy involves a progressive renal failure often accompanied by tubular atrophy and interstitial fibrosis [46], resulting in a chronic kidney disease (CKD). Kidney images were scanned with a Vectra microscope (Akoya Biosciences, MA, USA) at 10x magnification with a resolution of 1 µm per pixel. The selection of fields of view (FOV) from the whole slice was manually performed using the Vectra software (Phenochart 1.0.4) and images were generated with 20x magnification (0,5 µm per pixel). In one kidney section, 10 FOV were selected resulting in a total of 210 (sub-) Tiff images for the CKD data, for 21 individuals (8 pathological, 13 controls).

Heart and kidney tissues were fixed 24 hours in 4% formalin, transferred to 70% EtOH and paraffin embedded. Sections 4µm thick were deparaffinized, rehydrated and stained using Red Picrosirius in the automaton ST5020 (Leica Microsystems GmbH, Germany).

The presence of diffuse fibrosis in TTS and CKD was expected. Models with moderate fibrosis were chosen to place the software in challenging experimental settings where quantification is truly contributory. The software must therefore be sufficiently discriminating to identify moderate fibrosis rates, but also sufficiently stable to establish this identification in different use cases.

Comparison with ImageJ and inForm

Quantification of fibrosis rate obtained with FIBER-ML were compared with those obtained using of two other digital solutions: ImageJ1.8.0 (<https://imagej.nih.gov/ij/> , last date access December 01 2021) for cardiac data and inForm2.2 (Akoya Biosciences, MA, USA) for renal data.

ImageJ is a free software widely used by biologists [35,36] that allows the user to record procedures, or “macros” via a graphical interface. The macro used as a reference here was described by Hadi et al. in 2011 [37] and is currently used by biologists in research laboratories. A class, such as “fibrosis”, is defined by a region in the trichromatic space, defined by the ranges of hue, saturation and lightness, which are calculated from pixel red, green, and blue channels. These ranges were established manually using sliders on a training population of images.

InForm is a commercial software. InForm projects can be tailored to enable biomarker analysis in solid tissues and handle a variety of stains (H&E, multiplexed IHC, and multiplexed immunofluorescence). This software using trainable and automated algorithms enables detection, cell segmentation, tissue segmentation and identification of multiple markers within a sample. As well as FIBER-ML, it is based on a machine learning process [47]. The operator trains the algorithm by selecting classes in small regions of the images. It is generally sold as a complement to an acquisition device and, as far as we know, can only be run on proprietary format data.

All three software programs allowed to segment the fibrotic (f) tissue and the non-fibrotic (nf) tissue in order to deduce the *fibrosis rate*, defined as the ratio between the number of pixels of fibrosis (N_f) and the total number of tissue pixels, the sum of fibrosis and non-fibrosis ($N_f + N_{nf}$).

FIBER-ML results were compared with those from inForm for the renal data. Two operators (operator 1 and operator 2) performed two analyses each, one week apart on FIBER-ML, separately. One unique analysis was also performed by an independent user with inForm (operator 3).

FIBER-ML results were compared with those from ImageJ for the cardiac data. Concerning ImageJ, two operators performed the analyses (operator 1 and operator 2). With FIBER-ML, three operators (operators 1, 4 and 5) performed two analyses each one week apart, separately. Two operators (operators 4 and 5) were juniors, unfamiliar with histology.

Evaluation Criteria

Several metrics were used for intra-reader, inter-reader and inter-software comparisons: (a) the Pearson correlation coefficient r ; (b) the usual linear regression as a first approximation to the Passing Bablok regression [48,49]; (c) the Intraclass Correlation Coefficient (ICC) [49–51] which is a measure of agreement between two ratings and the discriminatory power (d), calculated as the p-value of the Mann-Whitney statistical test between healthy and pathological groups. To avoid overestimating the statistical power of the tests, the replicates were averaged in order to obtain a fibrosis rate value per animal, with a significance criterion of $p < 0.05$. ICCs were quoted according to Koo et al. [51]. 0 – 0.5: Poor; 0.5 – 0.75: Moderate; 0.75 – 0.9: Good; 0.9 – 1: Excellent.

Criteria were calculated for the different pairs of analyses. The whole analysis was summarized in a synthetic table, with minimum, maximum and average values. Comparisons of pairs of analyses were also represented graphically for illustrative purposes.

The time spent by the operator working actively with the software (supervised phase) and the total time spent by the software (including unsupervised phase) to provide the results were determined.

RESULTS

FIBER-ML

Process

The analysis process, illustrated in Fig.1, includes the following steps: (A) workspace definition and the identification of folders including the histological images; (B) learning/training of the algorithm, where the operator assigns a set of pixels to user-defined classes/categories (such as “fibrosis”); (C) application of the trained algorithm to all the images of a given study; (D) quality control including an evaluation form; (E) saving the summary of analysis and the evaluation form.

A representative sample of images must be chosen to define the learning dataset (Fig.1A). During the learning phase (Fig.1B), images are loaded one by one and the list of categories or “classes” (i.e. "Fibrosis," "Tissue" or "Background") are created, or loaded from another study. The operator selects the active class and chooses pixels corresponding to this class in the image by mouse clicks. Each mouse click enriches the learning list or "labeled dataset." The learning operation is iterated for each class and repeated on several images. For each click, the pixel intensity (red, green and blue) is associated with the class chosen by the operator. The graphical representation of the learning list is provided in a dedicated panel which shows a 3D trichromatic graph (Fig.1B), helping the operator to identify areas where he has not provided enough information to the software. A preview of the predicted classification map is available in fields of view (FOV) of the active image, allowing the operator to test and amend the learning list in an iterative way (Fig. 1B). Finally, the operator saves the learning list.

The classification model chosen for the fibrosis analysis was the discriminant analysis (DA) defined in the color space [52]. It is a fast and parsimonious statistical learning model (classifier) that assumes that the pixels of each class are roughly distributed as scattered ellipses (Gaussian mixture hypothesis). The DA algorithm establishes the parameters of the statistical model which fit the best

the learning list. The model then associates each pixel value (red, green, blue) with a class in line with the learning list (Fig. 1C). This association is performed point-to-point for all the pixels of all the images of the study. Of note, regions of interest (ROIs) in the images can be drawn to focus the analysis only on specific areas of the tissues.

The resulting class maps, or segmented images, are used for visual quality control, consisting in a comparative analysis between native and classified images on a visual interface (Fig. 1D). For each classification map, the operator can assign quality scores and a free comment that are to be saved in an Excel or CSV file.

The classification maps, the number of pixels of each class and the quality control scores are saved in a table (in Excel or CSV format) which summarizes the results of the calculated data (Fig. 1E).

Reproducibility

Intra- and inter-operator correlation (r) was high for both renal (CKD) and cardiac (TTS) data, with an overall mean of 0.98 ($p < 10^{-4}$) (Table1). Likewise, “excellent” [51] intra-operator agreements (ICC) were found, close to 0.95 for both CKD and TTS ($p < 10^{-4}$) (mean values in Table 1, illustration of pairs Fig.2A-B). “Good” values were observed for inter-operator ICCs, with a mean value of 0.76 ($p \leq 10^{-3}$) (Fig.2C-D), but with variabilities between pairs of analyses (Table 1). For renal data, it can be noted that operator 2 overestimates the fibrosis rate compared to the operator 1, resulting in a decrease in ICC (Fig.2B, 2D).

SOFTWARE COMPARISON

Fibrosis quantification of kidney data using FIBER-ML and inForm were highly correlated: $r = 0.96$ ($p < 10^{-4}$) (Table 1). Moderate to good agreements were observed between software programs: $ICC > 0.72$ for FIBER-ML 1.0 vs. ImageJ and $ICC > 0.8$ for FIBER-ML vs. inForm. Moreover, similar software discrimination capabilities were observed. As shown in Table 2, pathological CDK and TTS groups were statistically detected vs. healthy groups, whatever the program used, and, regardless of the software program used, the same orders of magnitude for the Discriminant values

were found: 10^{-3} for the cardiac data and 10^{-4} for the renal data (Table 2). Quantification of fibrosis rates produced significantly higher values with ImageJ than with FIBER-ML both in control and TTS group (Figure 3A). This difference did not have an impact on the discriminatory power.

FIBER-ML analyzed the dataset twice as fast as inForm for the kidney dataset, n=180 fields: 1.5 s vs. 3 s per image for FIBER-ML and inForm, respectively; and 4-5 times faster than ImageJ for the heart dataset, n=42 whole organ slices: 17s and 75 s per image for FIBER-ML and ImageJ respectively. During this process, FIBER-ML provided both individual segmentation maps (image by image) and a counting of the pixels of each class while ImageJ provided only the counting. ImageJ did not save classification maps or metadata. InForm saved metadata. FIBER-ML provided time-stamped traces of its calculations and metadata of the calculation parameters.

Qualitatively, operators reported FIBER-ML to be more user-friendly than ImageJ and to allow a better quality control. FIBER-ML was considered as user-friendly as inForm for generating fibrosis rates.

Visual Comparison

Visually, great similarities were found between most of the image segmentations (classifications) obtained with the different software, as illustrated Fig. 4A for FIBER-ML and ImageJ in the heart and Fig. 4B for FIBER-ML and inForm in the kidney. Slight segmentation differences between several FIBER-ML and ImageJ maps were observed especially on images where a low diffuse red staining in the tissues seemed to lead to overestimations of fibrosis by ImageJ (Supplemental Fig. S1). The images provided by inForm included a low-pass spatial filter (blurring) not included in FIBER-ML.

DISCUSSION

FIBER-ML allowed a robust, fast and user-friendly quantification of fibrosis rate in cardiac and renal tissue. The reproducibility of the FIBER-ML outcomes was assessed as well as their consistency with results obtained by two software often used by biologists and pathologists. High intra- and inter-operator correlations and high inter-software correlations were found in both heart and kidney datasets. All software solutions were sufficiently effective in detecting moderate fibrosis infiltrations in the order of 20% of the total tissue. The discrimination power between pathological and healthy groups were comparable between operators and software programs. Thus, FIBER-ML provided results similar to those available in ImageJ and inForm, but with a unique combination of ease of use, numerical efficiency and algorithmic transparency. Good intra-operator agreements were found. Inter-operator and inter-software agreements were moderate to good. The ranges of values obtained by different operators, or produced by different software, were comparable although this does not exclude possible slight biases. Comparison of fibrosis values between studies should be considered with relative caution and would require additional standardization steps based on operators consensus with respect to the classification of fibrosis.

High correlations

The r-correlation is a less restrictive metrics than ICC. ICC measures a strict equivalence between sets of results (type $y = x$) while the r-correlation indicates the extent to which the results are equivalent only to an affine relationship (type $y = a \cdot x + b$). Most statistical tests are invariant to this type of transformation, which ensures for example that a temperature test performed in °C remains valid in °F. Here, a high correlation (r) between two analyses indicated equivalent discriminant values (d) for the separation of disease and health groups, even if the ICC is not excellent. The discriminant values ($d < 0.01$) further confirmed that fibrosis rate measurements were effective enough to identify fibrosis rates in the 0% - 20% range. Correlation results are important since the

statistical differentiation between groups corresponds to the main use of quantification software. All the analyses were therefore consistent and statistically equivalent. Of note, this suggests that FIBER-ML can provide good results even when used by less experienced operators, after minimal training, although quality checks by a more experienced operator are strongly recommended.

Moderate to Excellent ICC

ICCs were calculated to evaluate agreements. (Table 1). Such a synthesis is not possible with visual Bland and Altman plots [50]. Overall, intra-operator ICCs were high. However, moderate ICCs generated by some operators were found (Fig. 2D), especially between experienced and novices with FIBER-ML. For the FIBER-ML vs. ImageJ comparison, ICCs, around 0.73 were considered moderate to good depending on whether the Cicchetti or Koo and Li assessment grid is used [53]. Generally, 0.75 is considered as the minimal value to define good agreements [51]. The ICCs were higher between FIBER-ML and inForm than with ImageJ. The orders of magnitude were globally preserved between analyses, notably between different operators and software. However, numerical values of fibrosis rates can slightly differ between analyses. Moderate differences are thus expected in particular between studies carried out by different teams. This suggests that for quantitative analyses of the fibrosis rate using a numerical software, it is necessary to design consensus meetings and supervision within teams, to share typical datasets and reference analyses between laboratories in order to improve normalization between teams.

Software Processes

FIBER-ML vs. ImageJ

ImageJ is a free on-line software which has been a reference of biological quantification for over 25 years [35]. In the present study, analyses were performed using an ImageJ plugin (a "macro") [37].

ImageJ and its macro was substantially less user-friendly than FIBER-ML. Implementations in ImageJ can vary from one laboratory to another according to the experience that local actors have of programming. As a result, neither the file management nor the traceability are currently optimal, as well as the tools for supervising the procedures. For example, no interface is proposed to select the (training) data allowing to set the parameters of the calculations (sliders). Similarly, no traces of intermediate results are provided. However, the great advantage of ImageJ and its main extensions comes from the fact that it is an old and stable platform, still active and widely shared, which assures the operator access to tools with proven robustness in the biological community. Thus, the high similitude between FIBER-ML and ImageJ outcomes are reassuring for the new FIBER-ML software insofar as ImageJ is a reference tool. Conversely, this similarity indicates that the improvement introduced by machine learning was probably marginal in terms of fibrosis rates. Concerning the marginal differences, several qualitative arguments tend to show that the differences would rather indicate an improvement of the analysis by FIBER-ML. A certain lack of specificity was observed on several images with ImageJ (Supplemental Figure S1). Moreover, a higher rate of fibrosis was observed in the control group for which no fibrosis is expected. Moreover, by construction, ImageJ considers that a pixel is “fibrotic” if it belongs to a geometrical shape box in the color space. This rather rigid approach introduces difficult compromises between what should be included in the box (sensitivity) and what should be excluded (specificity).

Moreover, FIBER-ML is easier to use than the ImageJ plugin, especially concerning the settings of calculations. With FIBER-ML, the decision is established step by step by a sequence of simple successive elementary decisions consisting in associating a pixel to a category. The ImageJ plugin requires to manage simultaneously six thresholds on colorimetric concepts that are not familiar to biologists. Moreover, with the ImageJ plugin, settings (learning), classification (production), and visual control are performed iteratively for each image of the study, while with FIBER-ML, learning, production and visual control are decoupled and the manual tasks can be performed

separately and split up to allow the operator to maintain attention. Hence, FIBER-ML can be used for the analysis of massive data, unlike the ImageJ plugin, since the plugin requires human resources in proportion to the volume of data to be processed.

FIBER-ML vs. inForm

The analysis process of FIBER-ML and inForm are comparable with a user-supervised learning phase followed by automatic classification of all images. InForm and FIBER-ML fibrosis rates were highly correlated and provided equivalent d-values. The comparison with inForm is interesting because inForm has reached a consensus among many pathologists. Kramer et al. showed high correlation between inForm and the evaluation of the pathologists (ground truth) in the measurement of areas of collagen deposition stained with Red Sirius in the hepatic tissue [47]. However, ICCs can vary from one operator to another, depending in particular on their experience of the interfaces of each software. The comparison of absolute values of fibrosis rates between software is therefore to be taken with caution.

FIBER-ML and inForm can measure biomarkers both in specific regions of interest and in whole tissue sections. InForm is used to recognize specific morphometric characteristics (size, shapes, proximity of the labeled regions, circularity, inclusion in another region) and different cell-type phenotypes, such as immune cells [54]. In its present version (1.0), FIBER-ML does not include these post-processing phases. However, post-processing can be performed easily from the classification maps provided by FIBER-ML in Tiff format, for each image of the study. InForm, like other commercial software, is not available in most of academic laboratories. In the version 2.2 of inForm, the source code is not accessible: only whole scans or fields with free dimensions can be used as input. Data must be in a proprietary format or to correspond to fields of pre-defined dimensions. In contrast, FIBER-ML is provided in two formats: a free executable format, and an open-source format that requires Matlab to run. FIBER-ML's algorithms are open-source and can be easily controlled and improved by the large Matlab community.

FIBER-ML Specificity

Supervised machine learning algorithms are particularly appropriate to integrate automation and human intervention. However, machine learning can introduce a great technical complexity that can lead to a loss of understanding and control of the process by the biologist. Moreover, the complexity of classification models requires increased resources to avoid instability (overlearning). The recourse to additional learning data to improve model stability is not always available and calls for human resources. Complex classifier models involve also more processing resources. A general histology data classification software should be designed to segment both targeted staining such as Sirius Red and non-targeted staining such as hematoxylin and eosin. In the case of non-specific staining, the information in the pixel is generally not sufficient to classify it and the local information around the pixel must be taken into account as well. To integrate this additional information, the algorithm adds to the native images several derived channels, obtained through filtering or texture maps. The amplification in dimension generate complexity to the classifier. Generalist software such as inForm, Genie or Ilastik [39,55] must therefore either use a complex classification model, even in simple cases of targeted staining, or ask the operator to dimension the complexity of the concern, which may be complex for a biologist. The increasing complexity of quantification algorithms for histology is often challenging to biologists and requires extensive software developments using resources that are essentially available in large-scale laboratories or companies. By narrowing the scope to specific staining, such as Sirius-Red, and being easy to use, FIBER-ML 1.0 can overcome these issues and offer a simple algorithm that is parsimonious in terms of human and machine resources. Moreover, operator's control and a reduction of the settings that can influence the final results of the process have been favored, according to recommendations of use [33]. In addition, generalist software, especially commercial ones, include complete workflows for targeted application sets. They can therefore integrate image preparation modules

(pre-processing) and shape and position analysis modules (post-processing), allowing for example to distinguish diffuse fibrosis from perivascular fibrosis [56]. However, predicting the main types of *research* applications which is not necessarily limited to fibrosis, is an overwhelming task. Therefore, FIBER-ML 1.0 has been designed as a modular open-access tool that manages the classification task only and can interface upstream and downstream with pre- and post-processing tools via TIFF inputs and outputs. This approach has the advantage to be freely modifiable by the community of users and developers in order to build a complete workflow and stable application library online.

Scope and limits

Presently on its present version, FIBER-ML supports targeted staining only. As with any supervised analysis algorithm, learning allows the classifier to be adapted to a specific context [57]. In the case of variable contexts within a study (staining quality, slice thickness), it is possible to normalize the data, perform separate trainings, exclude images, or try to use a consensus training. These important issues are outside the scope of this study, although the visual control module plays a key role to guide the choices of the operator. The evaluation of FIBER-ML was based on the analysis of data from two diffuse fibrosis models for which we had a high degree of control, and compared to two reference software. As for any software, the quality of analyses using FIBER-ML depends on the quality of the input data, and cannot be warranted when working on degraded data, e.g., low or inhomogeneous staining, or low-quality images, e.g., uncontrolled jpeg-type compression. Therefore, future users of FIBER-ML are strongly encouraged to use and abuse of the visual quality control for their own samples, as this is essential for the accuracy of the quantitative analysis. Future users are also encouraged to report results, difficulties, limitations, and to suggest improvements and modifications as indicated by clicking on the "about" button and on the public repository site. The openness of the software should favor more advanced analysis including scar fibrosis models, larger volumes of data, and comparisons with other reference software. Here, we

have shown the reliability of FIBER-ML for a particular application: Pricosirius Red staining for fibrosis rate assessment. The fibrosis rate can be assessed with other targeted stainings. As the pixel classes can be defined by the operator in the learning process, it is possible to use FIBER-ML with these other staining, in brightfied or fluorescence imaging. FIBER-ML 1.0 is presently tested in other staining including immune-histo-chemistry [40,42].

Conclusion

FIBER-ML 1.0 was able to distinguish healthy tissue from fibrotic one in the kidney and myocardium. The fibrosis quantification was comparable to two of the major software used in the biological research community, but combining user-friendly, open-source, parsimony and rapid execution. Thanks to the decoupling of operator time and on-the-fly calculations, FIBER-ML provides access to calculations on large volumes of data which should become an advantage in terms of reproducibility and statistical power.

Perspectives

The next objectives of FIBER-ML 1.0 are: (1) to reinforce the controls on the use of the software (help to detect atypical staining, include a test step between learning and production); (2) to facilitate the interfacing with the slide scanners (accept manufacturer format, management of large images usually causing memory overflow) and more importantly (3) to develop a community of users and contributors.

FIBER-ML 1.0 has been made freely at <https://gitlab.com/balvayda/fiber-ml> (last date access: January 11, 2022), under the GNU license.

ACKNOWLEDGMENTS

The authors are grateful to Corinne Lesaffre of the PARCC Histology Core Facility, Florence Marliot of the HEGP Histology Core Facility, and Patrick Bruneval for its enlightened opinions on the use of the software and the quality of the segmentation maps. Imaging was performed at the Imaging Facility (Plateforme d'Imageries du Vivant) of the University of Paris, supported by France Life Imaging (grant ANR-11-INBS-0006) and Infrastructures Biologie-Santé (IBISA).

References

- [1] Wynn T: Cellular and molecular mechanisms of fibrosis. *J. Pathol* 2008, 214(2):199–210.
- [2] Wynn TA: Fibrotic disease and the TH1/TH2 paradigm. *Nat Rev Immunol* 2004, 4(8):583–594.
- [3] Rockey DC, Bell PD, Hill JA: Fibrosis — A Common Pathway to Organ Injury and Failure. *N Engl J Med* (2015), 372(12):1138–1149.
- [4] Henderson NC, Rieder F, Wynn TA: Fibrosis: from mechanisms to medicines. *Nature* 2020, 587(7835):555–566.
- [5] Oliveira RS, de Barros BG, Gomes JM, Lobosco M, Alonso S, Bär M, dos Santos RV: Reactive Interstitial and Reparative Fibrosis as Substrates for Cardiac Ectopic Pacemakers and Reentries. *Bioinformatics and Biomedical Engineering - 4th International Conference, IWBBIO 2016, Granada, Spain, April 20-22, 2016, Proceedings. Edited by Ortuño Gizman FM, I. Rojas. Lecture Notes in Computer Science 9656, Springer 2016, ISBN 978-3-319-31743-4.*
- [6] Chemaly ER, Kang S, Zhang S, McCollum L, Chen J, Bénard L, Purushothaman K-R, Hajjar RJ, Lebeche D: Differential patterns of replacement and reactive fibrosis in pressure and volume overload are related to the propensity for ischaemia and involve resistin: Propensity for ischaemia, resistin and fibrosis in chronic loading. *J Physiol* 2013, 591(Pt21): 5337–5355.
- [7] Talman V, Ruskoaho H: Cardiac fibrosis in myocardial infarction—from repair and remodeling to regeneration. *Cell Tissue Res* 2016, 365(3):563–581.
- [8] Franjic B, Marwick TH: The diabetic, hypertensive heart: epidemiology and mechanisms of a very high-risk situation. *J Hum Hypertens* 2009, 23:709–717.
- [9] Díez J: Mechanisms of Cardiac Fibrosis in Hypertension, *J Clin Hypertension (Greenwich)* 2007, 9(7):546–550.

- [10] de Boer RA, De Keulenaer G, Bauersachs J, Brutsaert D, Cleland JG, Diez J, Du X-J, Ford P, Heinzel FR, Lipson KE, McDonagh T, Lopez-Andres N, Lunde IG, Lyon AR, Pollesello P, Prasad SK, Tocchetti CG, Mayr M, Sluijter JPG, Thum T, Tschöpe C, Zannad F, Zimmermann W-H, Ruschitzka F, Filippatos G, Lindsey ML, Maack C, Heymans S: Towards better definition, quantification and treatment of fibrosis in heart failure. A scientific roadmap by the Committee of Translational Research of the Heart Failure Association (HFA) of the European Society of Cardiology. *Eur J Heart Fail* 2019, 21:272–285.
- [11] Anderson L, Pennell D: The role of endomyocardial biopsy in the management of cardiovascular disease: a Scientific Statement from the American Heart Association, the American College of Cardiology, and the European Society of Cardiology. *Eur Heart J* 2008, 29(13):1696.
- [12] Boor P, Ostendorf T, Floege J: Renal fibrosis: novel insights into mechanisms and therapeutic targets. *Nat Rev Nephrol* 2010, 6(11):643–656.
- [13] Schoolwerth AC, Engelgau MM, Hostetter TH, Rufo KH, Chianchiano D, McClellan WM, Warnock DG, Vinicor F: Chronic Kidney Disease: A Public Health Problem That Needs a Public Health Action Plan. *Prev Chronic Dis* 2006 Apr, 3(2):A57. Available from URL: www.cdc.gov/pcd/issues/2006/apr/05_0105.htm.
- [14] Risdon RA, Sloper JC, De Wardener HE: Relationship between renal function and histological changes found in renal-biopsy specimens from patients with persistent glomerular nephritis. *Lancet* 1968, 2(7564):363–6.
- [15] Vilayur E, Harris DCH: Emerging therapies for chronic kidney disease: what is their role? *Nat Rev Nephrol* 2009, 5 (7):375–83.
- [16] Topham PS, Chen Y: Renal biopsy. *Comprehensive Clinical Nephrology*, 5th Edition. Edited by Johnson RJ, Feehally J, Floege J. Philadelphia, PA, Elsevier Saunders, 2010, pp. 75–81.

- [17] Berchtold L, Friedli I, Vallée J-P, Moll S, Martin P-Y, de Seigneux S: Diagnosis and assessment of renal fibrosis: the state of the art, *Swiss Med Wkly* 2017, 147:w14442. <https://doi.org/10.4414/smw.2017.14442>.
- [18] Fassett RG, Venuthurupalli SK, Gobe GC, Coombes JS, Cooper MA, Hoy WE: Biomarkers in chronic kidney disease: a review. *Kidney Int* 2011, 80(8):806–821.
- [19] Bamber J, Cosgrove D, Dietrich CF, Fromageau J, Bojunga J, Calliada F, Cantisani V, Correas J-M, D’Onofrio M, Drakonaki EE, Fink M, Friedrich-Rust M, Gilja OH, Havre RF, Jenssen C, Klauser AS, Ohlinger R, Saftoiu A, Schaefer F, Sporea I, Piscaglia F: EFSUMB Guidelines and Recommendations on the Clinical Use of Ultrasound Elastography. Part 1: Basic Principles and Technology. *Ultraschall Med* 2013, 34 (2):169–184.
- [20] Hueper K, Hensen B, Gutberlet M, Chen R, Hartung D, Barmeyer A, Meier M, Li W, Jang M-S, Mengel M, Wacker F, Rong S, Gueler F: Kidney Transplantation: Multiparametric Functional Magnetic Resonance Imaging for Assessment of Renal Allograft Pathophysiology in Mice. *Investig Radiol* 2016, 51(1):58–65.
- [21] Windisch P, Zwahlen DR, Koerber SA, Giesel FL, Debus J, Haberkorn U, Adeberg S: Clinical Results of Fibroblast Activation Protein (FAP) Specific PET and Implications for Radiotherapy Planning: Systematic Review. *Cancers (Basel)* 2020, 12(9):2629. <https://doi.org/10.3390/cancers12092629>.
- [22] Papadacci C, Finel V, Villemain O, Tanter M, Pernot M: 4D Ultrafast Ultrasound Imaging of Naturally Occurring Shear Waves in the Human Heart. *IEEE Trans Med Imaging* 2020, 39 (12): 4436–4444.
- [23] Farris AB, Alpers CE: What is the best way to measure renal fibrosis?: A pathologist’s perspective. *Kidney Int Suppl (2011)* 2014, 4(1): 9–15.
- [24] Istrătoaie O, Ofițeru A-M, Nicola G-C, Radu R-I, Florescu C, Mogoantă L, Streba CT: Myocardial interstitial fibrosis - histological and immunohistochemical aspects. *Rom J Morphol Embryol* 2015, 56(4):1473–80.

- [25] Ray PE, Liu XH, Robinson LR, Reid W, Xu L, Owens JW, Jones OD, Denaro F, Davis HG, Bryant JL: A novel HIV-1 transgenic rat model of childhood HIV-1-associated nephropathy. *Kidney International* 2003, 63:2242–2253.
- [26] Shao Y, Redfors B, Ståhlman M, Täng MS, Miljanovic A, Möllmann H, Troidl C, Szardien S, Hamm C, Nef H, Borén J, Omerovic E: A mouse model reveals an important role for catecholamine-induced lipotoxicity in the pathogenesis of stress-induced cardiomyopathy. *Eur J of Heart Fail* 2013, 15(1):9–22.
- [27] Rittié L: Method for Picrosirius Red-Polarization Detection of Collagen Fibers in Tissue Sections. *Methods Mol Biol* 2017, 1627:395-407.
- [28] Gurcan MN, Boucheron LE, Can A, Madabhushi A, Rajpoot NM, Yener B: Histopathological Image Analysis: A Review. *IEEE Rev Biomed Eng* 2009, 2:147–171.
- [29] Grimm PC, Computerized Image Analysis of Sirius Red-Stained Renal Allograft Biopsies as a Surrogate Marker to Predict Long-Term Allograft Function. *JASN* 2003, 14(6):1662–1668.
- [30] Schipke J, Brandenberger C, Rajces A, Manninger M, Alogna A, Post H, Mühlfeld C: Assessment of cardiac fibrosis: a morphometric method comparison for collagen quantification, *J Appl Physiol* 2017, 122:1019–1030.
- [31] Angell HK, Gray N, Womack C, Pritchard DI, Wilkinson RW, Cumberbatch M: Digital pattern recognition-based image analysis quantifies immune infiltrates in distinct tissue regions of colorectal cancer and identifies a metastatic phenotype. *Br J Cancer* 2013, 109(6):1618–1624.
- [32] Pavlides M, Birks J, Fryer E, Delaney D, Sarania N, Banerjee R, Neubauer S, Barnes E, Fleming KA, Wang LM: Interobserver Variability in Histologic Evaluation of Liver Fibrosis Using Categorical and Quantitative Scores. *Am J Clin Pathol* 2017, 147(4):364–369.
- [33] Aeffner F, Zarella MD, Buchbinder N, Bui MM, Goodman MR, Hartman DJ, Lujan GM, Molani MA, Parwani AV, Lillard K, Turner OC, Vemuri VNP, Yuil-Valdes AG, Bowman D:

Introduction to digital image analysis in whole-slide imaging: A white paper from the digital pathology association. *J Pathol Inform* 2019, 10:9.

- [34] Chauhan C, Gullapalli RR: Ethics of AI in Pathology: Current Paradigms and Emerging Issues. *Am J Pathol* 2021, 191(10): 1673-1683.
- [35] Schneider CA, Rasband WS, Eliceiri KW: NIH Image to ImageJ: 25 years of image analysis. *Nat Methods* 2012, 9(7):671-5.
- [36] Schindelin J, Rueden CT, Hiner MC, Eliceiri KW: The ImageJ ecosystem: An open platform for biomedical image analysis. *Mol Reprod Dev* 2015, 82(7-8):518–529.
- [37] Hadi AM, Mouchaers KTB, Schaliij I, Grunberg K, Meijer GA, Vonk-Noordegraaf A, van der Laarse WJ, Beliën JAM: Rapid quantification of myocardial fibrosis: a new macro-based automated analysis. *Cell Oncol* 2011, 34 (4):343–354.
- [38] Durkee MS, Abraham R, Clark MR, Giger ML: Artificial Intelligence and Cellular Segmentation in Tissue Microscopy Images. *Am J Pathol* 2021, 191(10):1693-1701.
- [39] Berg S, Kutra D, Kroeger T, Straehle CN, Kausler BX, Haubold C, Schiegg M, Ales J, Beier T, Rudy M, Eren K, Cervantes JI, Xu B, Beuttenmueller F, Wolny A, Zhang C, Koethe U, Hamprecht FA, Kreshuk A: ilastik: interactive machine learning for (bio)image analysis. *Nat Methods* 2019, 16:1226–1232.
- [40] Facchin C, Perez-Liva M, Garofalakis A, Viel T, Certain A, Balvay D, Yoganathan Y, Woszczyk J, De Sousa K, Sourdon J, Provost J, Tanter M, Lussey-Lepoutre C, Favier J, Tavitian B: Concurrent imaging of vascularization and metabolism in a mouse model of paraganglioma under anti-angiogenic treatment. *Theranostics* 2020, 10(8):3518–3532.
- [41] Sourdon J, Facchin C, Certain A, Viel T, Robin B, Lager F, Marchiol C, Balvay D, Yoganathan T, Favier J, Tharaux P-L, Dhaun N, Renault G, Tavitian B: Sunitinib-induced cardiac hypertrophy and the endothelin axis. *Theranostics* 2021, 11(8):3830–3838.
- [42] Sourdon J, Lager F, Viel T, Balvay D, Moorhouse R, Bennana E, Renault G, Tharaux P-L, Dhaun N, Tavitian B: Cardiac Metabolic Deregulation Induced by the Tyrosine Kinase

Receptor Inhibitor Sunitinib is rescued by Endothelin Receptor Antagonism. *Theranostics* 2017, 7(11):2757–2774.

- [43] Vassiliki' Coutsoumbas G, Gallo P, Zagnoni S, Di Pasquale G: Long-term injury after Takotsubo syndrome (stress cardiomyopathy). *Eur Heart J Suppl* 2020, 22(Suppl E):E73–E78. <https://doi.org/10.1093/eurheartj/suaa065>.
- [44] Gaillard F: Étude mécanistique de la fibrose interstitielle rénale et essai de preuve de concept thérapeutique Potent antiSTAT3 action in kidney by PPAR γ post-translational control of HIPK2. Thèse de doctorat, Sorbonne Paris Cité, 2018. Available from: <http://www.theses.fr/2018USPCB096>.
- [45] Sachdeva J, Dai W, Kloner RA: Functional and Histological Assessment of an Experimental Model of Takotsubo's Cardiomyopathy. *J Am Heart Assoc* 2014, 3(3):e000921. <https://doi.org/10.1161/JAHA.114.000921>.
- [46] Wyatt CM, Klotman PE, D'Agati VD: HIV-associated nephropathy: clinical presentation, pathology, and epidemiology in the era of antiretroviral therapy. *Semin Nephrol* 2008, 28(6):513–522.
- [47] Kramer AS, Latham B, Diepeveen LA, Mou L, Laurent GJ, Elsegood C, Ochoa-Callejero L, Yeoh GC: InForm software: a semi-automated research tool to identify presumptive human hepatic progenitor cells, and other histological features of pathological significance. *Sci Rep* 2018, 8:3418. <https://doi.org/10.1038/s41598-018-21757-4>.
- [48] Pum J: A practical guide to validation and verification of analytical methods in the clinical laboratory. *Adv Clin Chem* 2019, 90:215–281.
- [49] Patton N, Aslam T, Murray G: Statistical strategies to assess reliability in ophthalmology. *Eye (Lond)* 2006, 20(7):749–754.
- [50] Watson PF, Petrie A: Method agreement analysis: A review of correct methodology. *Theriogenology* 2010, 73(9):1167–1179.

- [51] Koo TK, Li MY: A Guideline of Selecting and Reporting Intraclass Correlation Coefficients for Reliability Research. *J Chiropr Med* 2016, 15 (2):155–163.
- [52] Nordhausen K: The Elements of Statistical Learning: Data Mining, Inference, and Prediction, Second Edition by Trevor Hastie, Robert Tibshirani, Jerome Friedman, *International Statistical Review* 2009, 77(3):482–482.
- [53] Cicchetti DV: Guidelines, criteria, and rules of thumb for evaluating normed and standardized assessment instruments in psychology. *Psychological Assessment* 1994, 6:284–290.
- [54] Granier C, Vinatier E, Colin E, Mandavit M, Dariane C, Verkarre V, Biard L, El Zein R, Lesaffre C, Galy-Fauroux I, Roussel H, De Guillebon E, Blanc C, Saldmann A, Badoual C, Gey A, Tartour É: Multiplexed Immunofluorescence Analysis and Quantification of Intratumoral PD-1⁺ Tim-3⁺ CD8⁺ T Cells. *JoVE* 2018, 132:56606. <https://doi.org/10.3791/56606>.
- [55] Daunoravicius D, Besusparis J, Zurauskas E, Laurinaviciene A, Bironaite D, Pankuweit S, Plancoulaine B, Herlin P, Bogomolovas J, Grabauskiene V, Laurinavicius A. Quantification of myocardial fibrosis by digital image analysis and interactive stereology. *Diagn Pathol.* 2014 Jun 9;9:114.
- [56] Courtoy GE, Leclercq I, Froidure A, Schiano G, Morelle J, Devuyst O, Huaux F, Bouzin C: Digital Image Analysis of Picrosirius Red Staining: A Robust Method for Multi-Organ Fibrosis Quantification and Characterization, *Biomolecules* 2020, 10(11):1585. <https://doi.org/10.3390/biom10111585>.
- [57] Cheng JY, Abel JT, Balis UGJ, McClintock DS, Pantanowitz L: Challenges in the Development, Deployment, and Regulation of Artificial Intelligence in Anatomic Pathology. *Am J Pathol* 2021, 191(10):1684–1692.

FIGURES LEGENDS

Figure 1. FIBER-ML 1.0 software overview. The FIBER-ML interface allows to launch the different stages of the analysis. **(A)** Selection or creation of a study (project) and loading of images into it. **(B)** Learning of the association between pixel colors and user-defined classes. **(C)** After a possible definition of regions of interest (ROIs), adjusting the classification model and applying it to the pixels of the study images to provide classification maps. **(D)** Visual inspection of data with optional completion of a quality form and **(E)** saving of the data summary.

Figure 2. Example of comparison between pairs of FIBER-ML quantifications performed by two operators. **(A,C)** Heart, **(B,D)** Kidney, **(A,B)** intra operator comparison (same operator, different readings), **(C,D)** inter user comparison (different operators, one reading). For each panel, the dots represent the mean value of all the sections for one mouse. Simple linear regression equation, correlation coefficient (r) and intraclass correlation coefficient (ICC) are shown.

Figure 3. Groups discrimination using FIBER-ML and a reference software. **(A)** Group comparison between FIBER-ML and ImageJ in cardiac sections. **(B)** Group comparison between FIBER-ML and inForm in kidney sections. Each dot corresponds to mean of fibrosis quantified for one mouse. Control groups (CTRL in blue) and disease groups (Takotsubo: TTS or nephropathy: CKD, in red) had different fibrosis rates. Mean bars with SEM are shown for each group. *** $p < 0.001$ and **** $p < 0.0001$ with Mann Whitney test between the control and disease groups for each software. Fibrosis rates are equivalent between FIBER-ML and inForm, but are higher using ImageJ compared to FIBER-ML. The difference of sensitivity in that case did not affect the statistical conclusions of the tests.

Figure 4. Comparison of classification maps obtained by FIBER-ML and other software. **A) complete slice of a myocardium (apex).** **Left**, classification map provided by ImageJ, fibrosis in black. **Center**, native image. **Right**, classification map provided by FIBER-ML, fibrosis in pink, background in white. **B) A field of kidney tissue.** **Left**, classification map provided by inForm, fibrosis in red, background in blue. **Center**, native image, a glomerulus is present near the center of the image. **Right**, classification map provided by FIBER-ML, fibrosis in pink, background in white.

TABLES

Correlation	r	r p-value	ICC	ICC p-value
Intra-user - FIBER-ML - TTS	0.988 [0.92 0.983]	< 10 ⁻⁴	0.969 [0.959 - 0.980]	< 10 ⁻⁴
Intra-user - FIBER-ML - CKD	0.979 [0.966 0.991]	< 10 ⁻⁴	0.940 [0.966 - 0.991]	< 10 ⁻⁴
Inter-user - FIBER-ML - TTS	0.979 [0.944 0.998]	< 10 ⁻⁴	0.829 [0.600 - 0.990]	0.001
Inter-user - FIBER-ML - CKD	0.977 [0.970 0.983]	< 10 ⁻⁴	0.683 [0.634 - 0.733]	0.0003
FIBER-ML vs. ImageJ - TTS	0.974 [0.960 0.974]	< 10 ⁻⁴	0.728 [0.588 - 0.789]	0.001
FIBER-ML vs. InForm - CKD	0.957 [0.917 0.978]	< 10 ⁻⁴	0.837 [0.664 - 0.971]	< 10 ⁻⁴

Table 1. Summary of the whole correlations analysis performed by multiple operators. Mean values of Pearson correlation coefficient (r), Intraclass Correlation Coefficient (ICC), ICC p-value are reported. Pearson correlation coefficient (r) and Intra-Class Correlations (ICC) are expressed as mean values [minimum maximum]. TTS: Takotsubo Syndrome, in heart; CKD: chronic kidney disease.

	Takotsubo	CKD
FIBER-ML	2.7 [1.7 - 6.0] 10^{-3}	1.8 [1.7 - 2.2] 10^{-4}
Image J	8.4 [1.7 - 25] 10^{-3}	n.a.
InForm	n.a.	3.9 [3.9 - 3.9] 10^{-4}

Table 2. Discriminant p-values (d-values). d-values are expressed as mean values [maximum minimum] among all quantification made; n.a. for not applicable.

FIBER INTERFACE

Help About

A DATA SELECTION
Select

Data

Stuy Data Select

Learn Data Select

B LEARNING

ROI

C PRODUCTION

D QUALITY

E SUMMARY

Processing on..

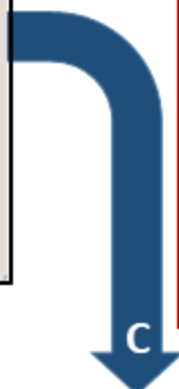
run untreated

ROI required

Quality sample

Num / Ratio 1

(Num > 1 / ratio <= 1)



CLASS

TISSUE

FIBROSIS

BACK-GROUND

Predicted classification

3D Trichromatic graph

Blue

Green

Red

Read Labels	Read Image	Read List	Remove Point	Control
Create Labels	Save Labels	Reset	Save List	Close

- ✓ STATUS
- ✓ IMAGE SCORE
- ✓ SEGMENTATION SCORE
- ✓ FREE NOTES

PIXEL INTENSITY

GREEN

BLUE

RED

Machine learning: Classification process for each pixel

Grey Yellow Pink

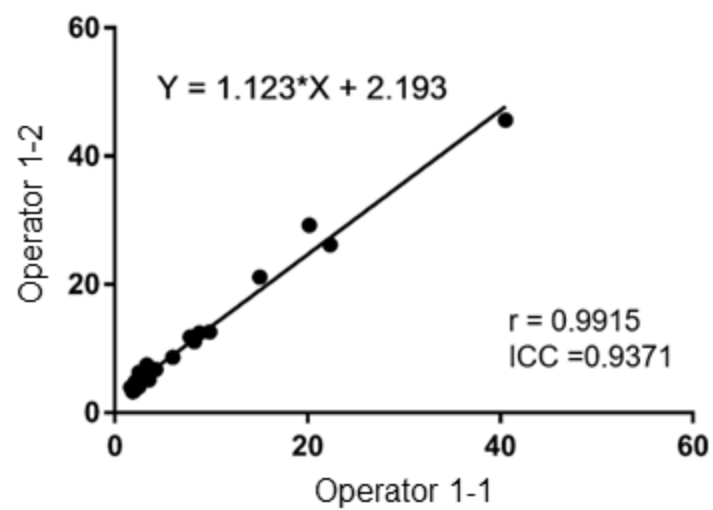
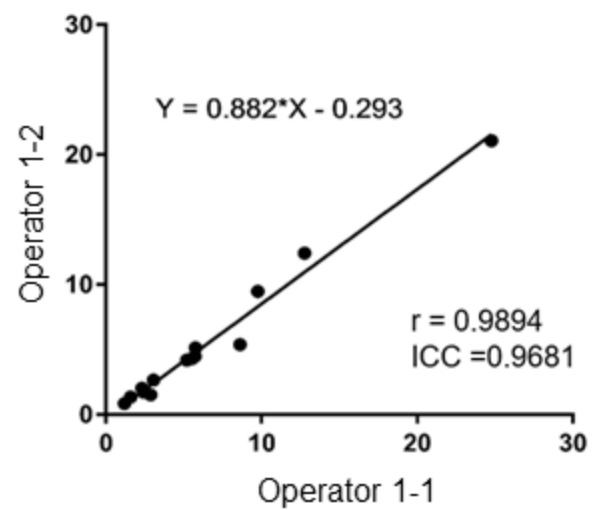
heart

kidney

A

B

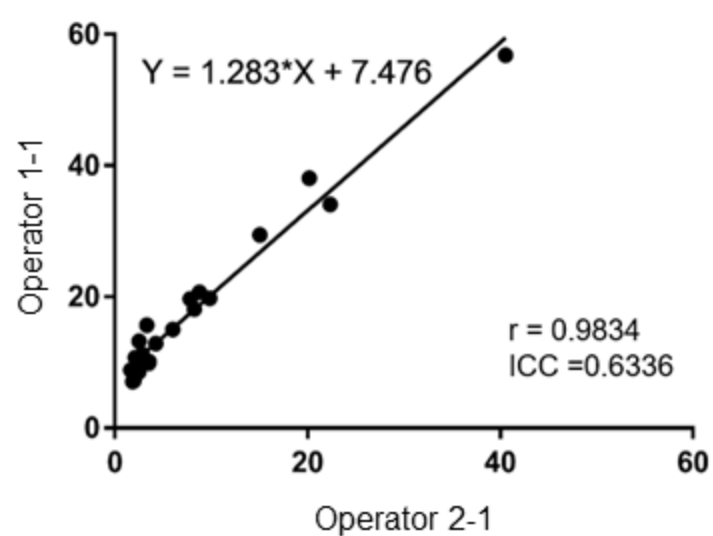
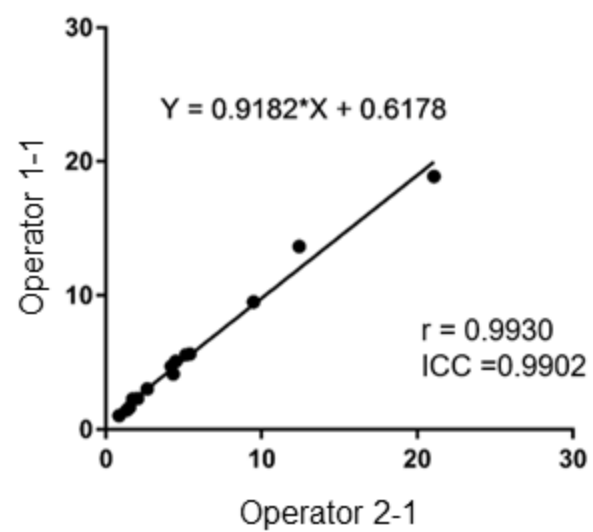
intra

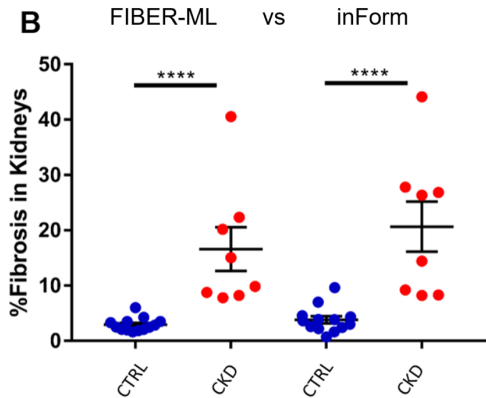
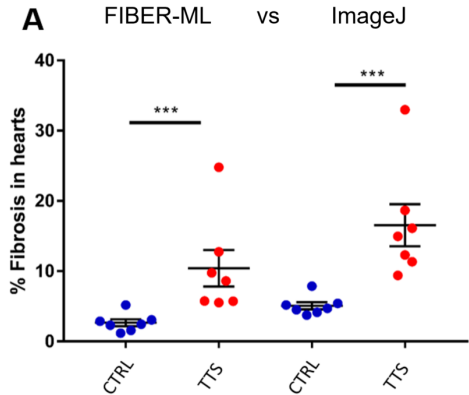


C

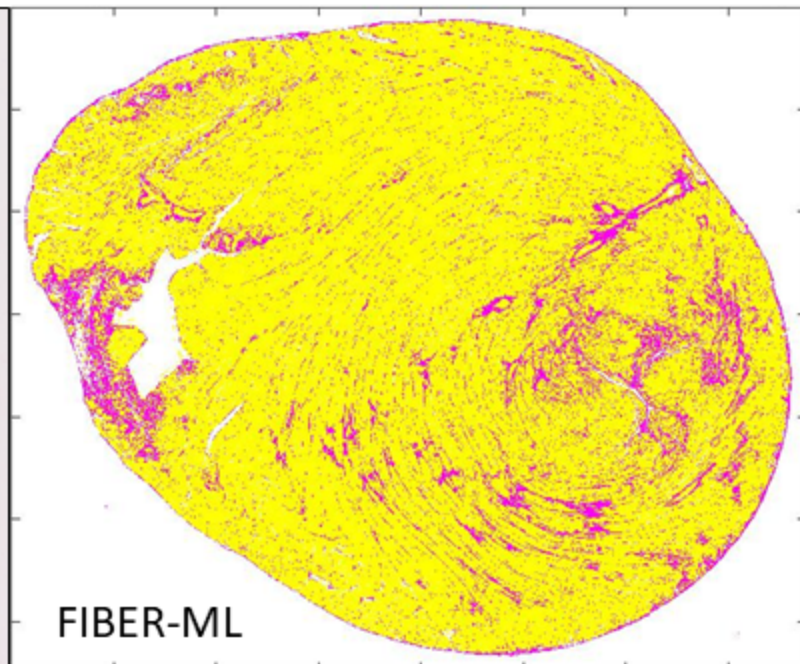
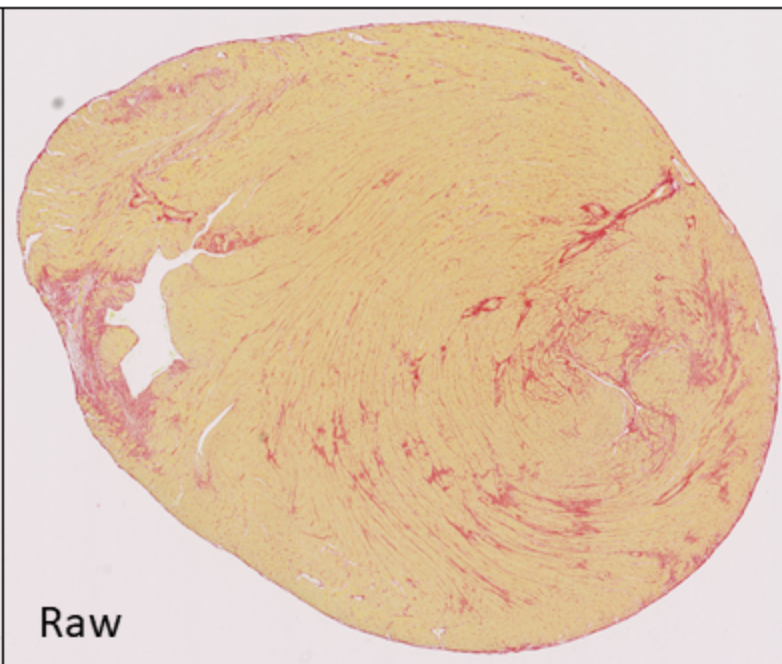
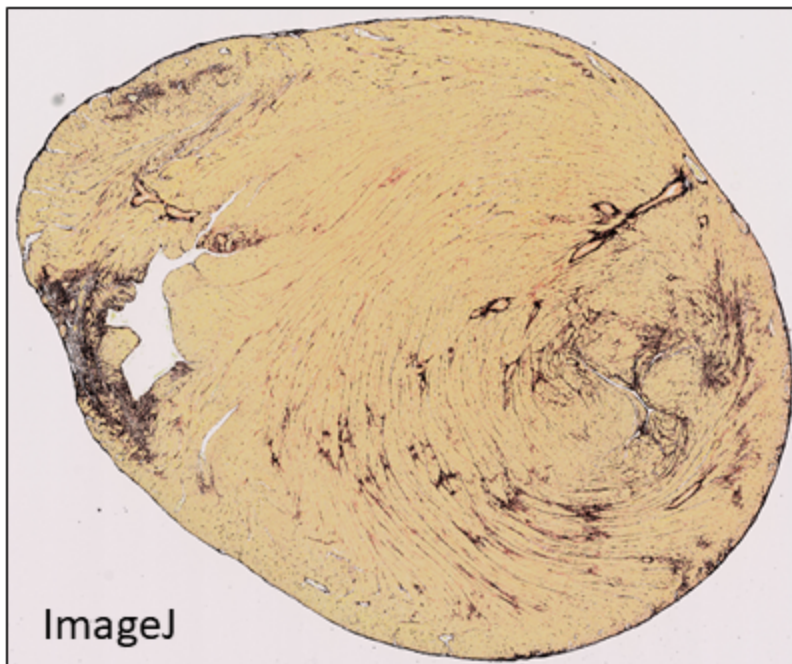
D

inter





A



B

